



Published in final edited form as:

Biophys Chem. 2018 July ; 238: 30–38. doi:10.1016/j.bpc.2018.04.004.

Predicting Neuroblastoma Using Developmental Signals and a Logic-Based Model

Jennifer C. Kasemeier-Kulesa¹, Santiago Schnell², Thomas Woolley³, Jennifer A. Spengler⁴, Jason A. Morrison¹, Mary C. McKinney¹, Irina Pushel¹, Lauren A. Wolfe⁵, and Paul M. Kulesa^{1,6,*}

¹Stowers Institute for Medical Research, Kansas City, MO, 64110, USA

²Department of Molecular & Integrative Physiology, University of Michigan Medical School, Ann Arbor, MI 48109, USA

³School of Mathematics, Cardiff University, Cathays, Cardiff, CF24, UK

⁴University of Pittsburgh School of Medicine, Pittsburgh, PA 15261, USA

⁵Fred Hutchinson Cancer Research Center, Seattle, WA 98109, USA

⁶Department of Anatomy and Cell Biology, University of Kansas School of Medicine, Kansas City, KS, 66160, USA

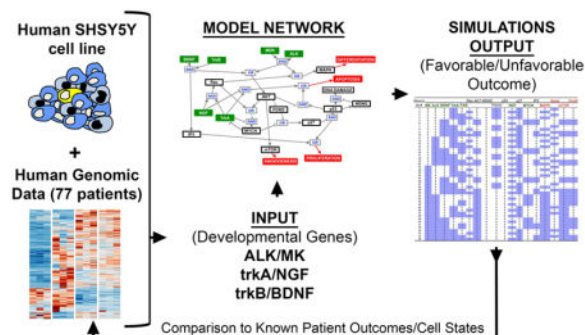
SUMMARY

Genomic information from human patient samples of pediatric neuroblastoma cancers and known outcomes have led to specific gene lists put forward as high risk for disease progression. However, the reliance on gene expression correlations rather than mechanistic insight has shown limited potential and suggests a critical need for molecular network models that better predict neuroblastoma progression. In this study, we construct and simulate a molecular network of developmental genes and downstream signals in a 6-gene input logic model that predicts a favorable/unfavorable outcome based on the outcome of the four cell states including cell differentiation, proliferation, apoptosis, and angiogenesis. We simulate the mis-expression of the tyrosine receptor kinases, *trkA* and *trkB*, two prognostic indicators of neuroblastoma, and find differences in the number and probability distribution of steady state outcomes. We validate the mechanistic model assumptions using RNAseq of the SHSY5Y human neuroblastoma cell line to define the input states and confirm the predicted outcome with antibody staining. Lastly, we apply input gene signatures from 77 published human patient samples and show that our model makes more accurate disease outcome predictions for early stage disease than any current neuroblastoma gene list. These findings highlight the predictive strength of a logic-based model based on developmental genes and offer a better understanding of the molecular network interactions during neuroblastoma disease progression.

Graphical Abstract

*Address correspondence to: Paul M. Kulesa, Ph.D., Stowers Institute for Medical Research, 1000 East 50th St, Kansas City, Missouri, 64110. Tel. (816) 926-4314; Fax (816) 926-2074; pmk@stowers.org.

The authors declare no potential conflicts of interest



Keywords

neuroblastoma; trkB; logic model; molecular network

INTRODUCTION

Neuroblastoma is a pediatric, often fatal tumor of the sympathetic nervous system derived from embryonic neural crest cells that fail to properly migrate and differentiate. Prognosis in children is typically based on age at diagnosis, stage, histology, chromosomal aberrations and amplification of the N-myc proto-oncogene MYCN. In addition, the comparison of published gene expression patterns from human neuroblastoma patient-derived tissues have produced sets of high risk genes put forward as prognostic indicators of disease outcome (1–8). However, this approach has shown limited prognostic potential since it is based on the correlation of gene expression profiles of effectual rather than causal genes. Thus, there is a critical need for better predictive models of neuroblastoma progression and disease outcome that are based on the developmental gene and signaling pathways involved in neuroblastoma pathogenesis.

During embryonic development multipotent trunk neural crest cells migrate ventral and differentiate into neurons to assemble the sympathetic nervous system (SNS). Sympathetic neurons regulate several biological processes including heart rate and blood pressure, and the fight or flight response (9). But, mistakes in developmental signals that direct neural crest cells to precise locations and regulate cell differentiation may lead to neuroblastoma pathogenesis. Recently, we discovered a crucial role for the receptor tyrosine kinase, trkB and its ligand brain-derived neurotrophic factor (BDNF) to direct trunk neural crest cells in chick to ventral sites during SNS formation (10). When trkB is blocked or BDNF secretion is inhibited by microsurgery, or chemically, neural crest cells fail to migrate to the secondary and final location of the sympathetic ganglia. The microenvironmental signals that initiate the neural crest cell migration and regulate trkB expression during SNS development remain unclear but provide a molecular inroad to neuroblastoma pathogenesis.

Intriguingly, trkB is a well-established marker of poor human neuroblastoma prognosis, with approximately 36% of neuroblastoma cells expressing trkB (11, 12). In addition, another receptor tyrosine kinase anaplastic lymphoma kinase (ALK) regulates the proliferation of immature sympathetic neurons (13). ALK has been shown to be mutated in 6–10% of

neuroblastoma tumors (14, 15). Lastly, MYCN overexpression combined with activated ALK is sufficient to induce the neuroblastoma phenotype in mouse sympathoadrenal cells (16). In contrast, another family member, trkA, is a good prognosis marker and is preferentially expressed by neuroblastoma tumors that naturally regress (17). Thus, receptor tyrosine kinase signaling is critical to normal sympathetic nervous system development, but it remains unclear how the dysregulation of an underlying molecular network leads to neuroblastoma pathogenesis.

Computational methods, such as discrete Boolean logic (18) have emerged as a means to rapidly identify the regulatory structure of dysregulated networks that would enable the rational development of more precise therapeutic avenues. For example, Wynn and colleagues (19) develop a network model of Notch signaling in colon cancer using a novel reverse engineering Boolean-based method and discover potential mechanisms of action for honokiol as an anti-cancer drug. Boolean models are also specifically suited to capturing the qualitative features of interacting components, such as T cell receptor signaling, cell cycle transition between the G1/S phases and hepatocellular specification (20–23). Equally, stationary states of Boolean networks have been used to understand how distinct phenotypes arise in many developing systems (24–27). Thus, logic-based models based on specific disease signaling networks may lead to a predictive tool for more informed prognoses.

Here, we asked whether a signaling network that includes trkA and trkB signaling more accurately assesses the biological activity of neuroblastoma cells and thus better predicts neuroblastoma disease progression. We also asked to what extent the down-regulation of trkB or the over-expression of trkA would alter the outcome of neuroblastoma progression. To address these questions, we constructed a logic-based model based on receptor tyrosine kinase signaling trkA, trkB, and ALK to predict 4 key states of neuroblastoma: differentiation, apoptosis, angiogenesis, and proliferation. To test the predictive value of our model, we collected the transcriptomic signature of the human neuroblastoma cell line SHSY5Y and confirmed the input genes by antibody staining. We then predicted which steady state outcomes of the logic-based model map to the 6-gene input signature of the SHSY5Y cell line. We then confirm the predicted states on SHSY5Y using antibody labeling. Lastly, to address the relevance of our studies to the human disease population, we gathered the 6 input gene states from 77 patient-derived samples with known outcomes (28) and let the model predict a favorable versus unfavorable outcome for comparison. Our results offer a detailed picture of the molecular interactions of receptor tyrosine kinase signaling in neuroblastoma and provide a framework for linking genomic profiling data with neuroblastoma disease progression.

MATERIALS AND METHODS

Logic network model construction

To begin to construct a logic based model of neuroblastoma, we focused on normal developmental signaling pathways of sympathetic neurogenesis centered around tyrosine receptor kinase (trk) receptors/ligands and downstream signals and curated data from the published literature. Based on these data, we constructed a biological signaling network of developmental genes (involved in sympathetic neurogenesis and neuroblastoma) and adapted

the approach used in (29) to convert the molecular interactions into logical functions using known outcomes. That is, developmental genes were represented as either active or inactive and the dynamics of the system evolved from downstream interactions of components (e.g., feed forward, feedback) that resulted in a particular outcome(s) (e.g., proliferation, apoptosis, differentiation, vasculogenesis). We considered all four outcomes biologically compatible and consistent with our hypothesis that uncontrolled signaling events during normal sympathoadrenal development leads to neuroblastoma progression. The initial model was simulated and verified that there were no contradictions with current literature.

Logic network model simulation and data post-processing

The 18 inputs were initially fixed to some combination of zeros and ones. Specifically, for completeness, we considered all 2^{18} possible initial configurations, from (000...000) to (111...111). For each initial condition the network rules from Figure 1B were applied to the initial states, and the states were updated synchronously to their new values. The application of the network rules was repeated until either the system reached a steady state, or the system began to oscillate. After all 2^{18} simulations had terminated we tallied all the simulations that ended in a steady state and all of those that oscillated and divided these numbers by 2^{18} . These ratios are the probabilities that any uniformly randomly generated input would lead to either a steady state, or an oscillatory state. Since there were very few final oscillatory, or steady states we were further able to analyze each state individually. Specifically, for each steady state, we tallied how many initial conditions led to that steady state and divided this number by the total number of initial conditions that led to any steady state to provide a conditional probability. Namely, given that a state is stable, this ratio is the probability that it is a specific steady state. The oscillatory states were treated similarly, in that we tallied up all the initial conditions that led to a particular oscillatory state and divided this number by the total number of initial conditions that led to any oscillatory state. In the case that a particular input was fixed on, or off, the procedure is practically identical to the above description. However, we note that the system is run with fewer inputs to account for the fixed setting. Equally, the network structure was altered to ensure that each iteration did not change the fixed value.

Discretization of Data

Because logic models are qualitative models based on digital signals, they are well suited for qualitative data. A two-state logic model assumes that for each node in a network, there is a threshold above which the node is active (ON) and below which it is mostly inactive (OFF). To determine these input states for our SHSY5Y human neuroblastoma cell line, we separately stained cells for MDK, ALK, BDNF, trkA, trkB, NGF. The model output parameters were determined by protein labeling for differentiation-TuJ1 (30), apoptosis-caspase3 (31), angiogenesis-mTOR (32), proliferation-H3 (33). In order for a protein to be considered ON using antibody expression analysis, in an experimental condition, the total signal for the protein in a given condition was expressed by at least 50% of the cells analyzed.

Human SHSY5Y neuroblastoma cell line

The human SHSY5Y neuroblastoma cell line was obtained from ATCC (CRL-2266) and maintained in 1:1 mixture of Eagles's Minimum Essential Medium (ATCC, 30-2003) supplemented with 10% FBS (VWR, 97068-085). Cells were plated in 8-well chamber slides (ThermoFisher, 177402) for Immunohistochemistry. All cultures were determined to be free of mycoplasma contamination using a polymerase chain reaction-based detection system (Roche, 0518424001).

Immunohistochemistry

Cultured cells were fixed in 4% PFA for 20min. Immunocytochemistry on fixed cells were processed as in (34) and (35). Primary antibodies included: Midkine (MDK; ThermoFisher, PA5-19640), ALK (Cell Signaling Technologies, 3633), BDNF (ThermoFisher, OSB00017W), trkB (Santa Cruz, sc-377218), trkA (Cell Signaling Technologies, 2505), NGF (Cell Signaling Technologies, 2046), Tuj1 (R and D Systems, MAB1195), Caspase3 (Cell Signaling Technologies, 9662), mTOR (ThermoFisher, PA5-518) and H3 (Novus Biologicals, NB100-747).

RNA-seq of SHSY5Y neuroblastoma cell line

Total RNA was isolated from three, separate T25 flasks of adherent SHSY5Y cells at approximately 60% confluency using Sigma's GenElute mammalian Total RNA miniprep kit (Millipore Sigma, RTN70) per the manufacturer's recommendations. Total RNA was quantified on an Agilent Bioanalyzer 2100 using a Eukaryote Total RNA Nano chip (Agilent, 5067-1511) as well as a Nanodrop spectrophotometer (ThermoFisher Scientific, ND-1000). Libraries were made from 500ng of total RNA according to the manufacturer's directions for the TruSeq Stranded mRNA LT– set A and B (Illumina, Cat. No. RS-122-2101 and RS-122-2102) kit. Resulting short fragment libraries were checked for quality and quantity using the Bioanalyzer High Sensitivity DNA assay (Agilent; 5067-4626) and Qubit Fluorometer (Life Technologies). Libraries were pooled, re-quantified and sequenced as 50 base pair, single reads on the Illumina HiSeq 2500 instrument to a depth of at least 20 million reads per sample using HiSeq Control Software 2.2.58.

Bioinformatics analysis

Following sequencing, Illumina Primary Analysis version RTA 1.18.64 and bcl2fastq2 were run to demultiplex reads for all libraries and generate FASTQ files. FASTQ files were mapped to the human genome hg38 from UCSC using Tophat (2.1.1) with options – segment-mismatches 1 -x 1 -g 1. Ensembl 87 annotations were used to define gene coordinates. Quality of the samples was assessed using FastQC (0.10.1). The R (3.3.1) environment was employed for the statistical analysis of the data. RPKM values were found using edgeR (3.12.0).

Confocal Imaging

Images were collected on an inverted laser scanning confocal microscope (LSM5 Pascal, Carl Zeiss, Thornwood, NY) using either a Plan-Neofluar 10X/0.3, Plan-Neofluar 40X/0.75 or C-Apochromat 40X/1.2W objective (Carl Zeiss, Thornwood, NY). The GapYFP was

excited with the 488 nm laser line using the FITC filter and all other imaging parameters were as described in (36). Images were collected, processed and analyzed using AIM software (Carl Zeiss, Thornwood, NY).

Human Neuroblastoma patient data and logic model comparison

Patient data was taken from (28). All data is publicly available on the NCBI Gene Expression Omnibus (<https://www.ncbi.nlm.nih.gov/geo/>, GSE3960). Raw CEL files were downloaded and processed using the R package affy (version 1.50.0). Presence or absence of a gene was determined using the mas5calls function. This performs a Wilcoxon signed rank-based gene expression detection algorithm that was first used in Affymetrix Microarray Suite version 5. A table was then generated of the expression (presence or absence) of the 6 input genes: MDK, ALK, trkA, NGF, trkB and BDNF with outcome status for each patient. For each patient sample, the input genes status was aligned to the logic model predictions and a steady state was assigned and compared to the actual patient outcome from (28). That is, we did not convert the scoring used by Wang et al (28) into a phenotypic output. The logic model outcomes of Differentiation, Angiogenesis, Proliferation and Apoptosis were categorized as good, poor or intermediate outcome. Histological characteristics and prognosis assignments were taken from cancer.gov assignments for neuroblastoma of proliferation as unfavorable (apoptosis as favorable) and differentiation as favorable. Additionally, angiogenesis is given a poor outcome based on (37). Based on how many outcomes the model predicts as ON or OFF, the sum of outcomes is categorized i.e. 2 good outcomes and 1 poor outcome would give an overall intermediate outcome. If the sum of the good and poor outcomes is equal, an intermediate outcome is assigned.

RESULTS

Model development of a neuroblastoma interaction network based on receptor tyrosine kinase and downstream signals

Some signals in neuroblastoma disease progression have been identified, however their precise molecular interactions are unclear. This includes the receptor tyrosine kinase family of signaling molecules, such as trkA and trkB that more recently have been shown to play important roles in sympathetic nervous system development. The molecular interactions of these signals may be specified as active, or inhibitory, but definite rate parameters are missing. Thus, instead of considering the temporal evolution of the molecular concentrations, the interaction network may be abstracted as a Boolean network with genes and signals in one of two possible expression states: active (1 or ON) or inactive (0 or OFF). This provides a general idea of activation states that can be logically maintained (30) that in turn suggest favorable or unfavorable outcomes associated with disease progression.

To address this, we constructed a logic network based on trkA, trkB, and ALK signaling that contains 16 species; 3 out of the 16 species are pure input parameters, including ALK, Midkine (MDK), and Nerve Growth Factor (NGF) (Fig. 1A, B). There are four outputs from the network that predict the outcomes of differentiation, proliferation, angiogenesis, and apoptosis. These include: (1) MAPK, a reporter of cell differentiation based on several studies of neuroblastoma differentiation (38,39,40,41) and normal receptor tyrosine kinase

signaling (42,43); (2) mTOR, was selected as a reporter of angiogenesis from studies in neuroblastoma (44,45,46) and as a target of anti-angiogenesis drug therapies (47,48), and; (3–4) Apop and Prolif, reporters of apoptosis and cell proliferation, respectively (Fig. 1A, B). The logic functions are explicitly indicated and biologically justified (Table 1).

There are 262,144 (2^{18}) possible states for the network. However, most of these states are unstable and will transition to other states as the network rules are applied through synchronous iteration. The applied rules are represented by AND, OR and NOT interactions illustrated in Figure 1B. These interactions were obtained by a systemic analysis of the literature following the approach proposed in (29). Since there are nearly 300,000 possible states, randomly generating initial conditions will lead to a lot of wasted effort and reproduction of states. Thus, we simulated all states once and then collated the information from all possible different states. Although this seems like a large number of simulations the network state rapidly tends to a steady or oscillatory state after a small number of iterations. Using a parallelized approach, all 2^{18} initial conditions can be simulated in just over two minutes.

Model simulations show that all initial conditions terminated in a steady state with p27 and trkA in synchrony in 70% of outcomes

Model simulations show that from random initial conditions the simulations are most likely to converge to a steady state in nearly 70% of simulations (Fig. 1C); including to one of 9 steady states (Fig. 1C, Supplementary Fig. S1; steady state numbers 1, 3, 7, 11, 13, 17, 21, 23, 27) with a combined total of approximately 30% probability; and to a lesser extent to converge to one of 9 steady states with approximately 20% (Fig. 1C, Supplementary Fig. S1; steady state numbers 2, 4, 8, 12, 14, 18, 22, 24, 28). We observed that p27 (an indicator of cell cycle inhibition) expression exactly matches trkA expression at 32 out of 46 of the steady states (Supplementary Fig. S1). That is, p27 is activated if, and only if, trkA is activated (Supplementary Fig. S1). Also, AKT, IP3, mTOR and Proliferation expression all match one another at steady state (Supplementary Fig. S1). For example, steady state number 33 has AKT = mTOR = Proliferation = 1, but IP3 = 0 (Supplementary Fig. S1). AKT and mTOR track one another, but not IP3 or Proliferation (Supplementary Fig. S1). Interestingly, there is only 1 out of 46 steady states in which MAPK, Apop, mTOR and Prolif are all activated (Fig. 1C, Supplementary Fig. S1; steady state number 45). This implies that the four outcomes including Angiogenesis, Proliferation, Differentiation and Apoptosis all occur in this steady state. However, this steady state (Supplementary Fig. S1; number 45) is only reachable around 1% of the time from uniformly random initial conditions and is thus a very rare event (Fig. 1C, Supplementary Fig. S1). Moreover, it should be noted that Apoptosis, mTOR and Proliferation are only active together in 4 out of 46 steady states (Fig. 1C, Supplementary Fig. S1; 9, 19, 29, 45; with a combined probability of 4%). Thus, the probability of reaching a state where 3 or 4 out of outcomes are all active is very low.

Continuous overexpression of trkB by fixing trkB 'ON' reduced the number of steady states and led to fewer favorable outcomes

To address how the model network reacts to changes in trkB, we initially overexpressed trkB in silico by fixing trkB to be 'ON' as an initial input in the model (Fig. 2A, B). When trkB is fixed 'ON', the model predicts a reduction in the number of steady states to 26 from 46, compared to the wildtype network (Fig. 2A, B). There are 6 out of 26 steady states with the highest probability (Fig. 2B; steady state numbers 1,2,7,8,13 and 14) of occurrence (30%) and correlate with high FOXO expression (neuroblastoma differentiation state; (37)) and low AKT and IP3 expression (Supplementary Fig. S2). We also observe that forcing trkB 'ON' shifts towards more poor outcomes as compared to the wildtype network (37% good, 53% poor, and 10% intermediate). Furthermore, when trkB is fixed 'ON', the model network predicts only favorable outcomes with Apoptosis (Supplementary Fig. S2; steady states 1,7,13) or Differentiation (Supplementary Fig. S2; steady states 2,8,14) in 3 out of 26 of the steady states with 11% probability of occurrence (Supplementary Fig. S2).

Knockdown of trkB by fixing trkB 'OFF' led to more favorable disease outcomes

When trkB is knocked down by fixing trkB to 'OFF' in the model, there is an increase in the probability of ending in a steady state (70%; Fig. 2A) and there are fewer steady states than compared with the trkB 'ON' simulations (Fig. 2B, C). With trkB fixed 'OFF', the model predicts that the steady states with the highest probability of occurrence (Fig. 2C; steady states 1–12) correlate with high FOXO expression and low AKT expression (differentiation). Steady states 1,3,5,7,9,11 (~36% probability of occurrence) all show Apoptosis 'ON' and steady states 2,4,6,8,10,12 (21% probability of occurrence) all show MAPK 'ON' (Fig. 2C, Supplementary Fig. S3). Therefore, by forcing trkB 'OFF', as should occur during normal sympathoadrenal development we see a dramatic increase in good outcome states (Supplementary Fig. S3; 79% good, 4% bad, 17% intermediate).

Continuous overexpression of trkA by fixing trkA 'ON' led to dramatic changes in the number of steady states and a favorable outcome in 75% of all simulations

When we simulated the model network with trkA 'ON', there was a significant increase in the probability of ending in a given steady state to 100% (Fig. 2A) and a reduced number of steady states (Fig. 2D; 32 steady states) compared to the wildtype network (Fig. 1C). All 32 steady states have the same probability of occurring (Fig. 2D) and 24 out of 32 steady states produced a favorable outcome (Supplementary Fig. S4; 75%). Interestingly, trkA 'ON' only produced states with MYCN 'OFF' (Supplementary Fig. S4), a correlation not observed in other simulations, suggesting a possible link between non-amplified MYCN tumors and spontaneous regression through trkA expression.

The model accurately predicted a steady state outcome with the human SHSY5Y neuroblastoma cell line

To test our model network with a realistic scenario, we took advantage of the human SHSY5Y neuroblastoma cell line. In order to define the state (ON or OFF) of the 6-gene input (ALK/MDK, trkA/NGF, trkB/BDNF), we generated an RNAseq transcriptional profile of the SHSY5Y cell line (Supplemental Information). We further confirmed our RNAseq

data by immunolabeling the SHSY5Y cells for protein expression of the 6-gene inputs (Fig. 3). Since the logic model is based on single cells, in order to take the population of cells into consideration we assigned an input gene to be 'OFF' if it was expressed in less than 50% of the population and 'ON' if expressed in greater than 50% (Fig. 3). In the SHSY5Y cell line, we found ALK/MDK, trkA/trkB/NGF to be 'ON' and BDNF, 'OFF' (Fig. 3). Based on this, the SHSY5Y input genes align to one of the logic model steady states (Fig. 3; steady state number 38). This predicts an outcome in which Differentiation and Angiogenesis are 'ON' and Apoptosis and Proliferation are 'OFF' (Fig. 3). To determine whether this predicted outcome is a steady state of the SHSY5Y cell line, we examined the 4 outcome states by protein expression and confirmed that the SHSY5Y cells are >50% TuJ1-positive (Differentiation 'ON') and mTOR-positive (Angiogenesis 'ON'), and <50% caspase3-negative (Apoptosis 'OFF') and H3-negative (Proliferation 'OFF') (Fig. 3). Thus, our model accurately predicted the steady state outcome of a human neuroblastoma cell line based on a 6-gene input signature.

The model predicted the outcomes of 77 human neuroblastoma patient samples and is highly accurate in the case of children less than two years of age

To broaden our model application and test its accuracy to predict the outcomes of human patient data, we extracted the 6-gene input signatures from published neuroblastoma patient samples (n=77 patients) with known clinical outcomes (28) (Fig. 4A). Each patient sample 6-gene input signature was aligned to the wildtype network (Fig. 4). Based on the outcomes from the model predictions, a favorable or unfavorable result for each patient was assigned (Fig. 4). We then compared our results to the clinical outcomes (28), alive or succumbed. That is, our criteria for calling "correctly predicted" by the simulations was a match of either 'favorable' prediction with 'alive' clinical outcome or 'unfavorable' prediction with 'succumbed' clinical outcome (28). Of the 77 patient samples analyzed, our model correctly predicted the clinical state approximately 80% of the time (Fig. 4). Interestingly, when we subcategorized the patient sample results, the model correctly predicted the outcome of neuroblastoma stages 1–3, International Neuroblastoma Staging System (INSS), 100% of the time (Fig. 4B). Of patient's less than one-year of age, we observed a 96% correct prediction rate and in children less than 2 years of age, a 91% correct prediction rate (Fig. 4C). In contrast, we only see a 55% correct prediction rate in patients over 4 years of age (Fig. 4B). Thus, our logic model was able predict the outcome of younger neuroblastoma patients (<2 yrs of age) with high accuracy.

DISCUSSION

We were motivated to perform this study by the lack of information about the molecular circuitry underlying neuroblastoma disease progression and inefficient predictive capabilities of current models. Without this information, therapy strategies developed in conjunction with initial diagnoses rely on a historical and general set of criteria that may or may not result in an individual patient's favorable outcome. Furthermore, models based on gene expression correlations between neuroblastoma patient samples have shown that pooling information from as many as 23 published signatures does not improve the accuracy of predicting a favorable or unfavorable disease outcome (50). By constructing a logic model

network based on developmental genes and signaling pathways, including the receptor tyrosine kinase family, we suggest our results offer unique insights into the molecular network of neuroblastoma pathogenesis and a better predictive tool to assess human patient disease progression.

Our logic-based model was constructed with a 6-gene input signature based on genes involved in sympathetic nervous system development (ALK/MDK, trkA/NGF, trkB/BDNF). By centering our predictions on the biological signaling features of receptor tyrosine kinase signals rather than on an array of effectual genes derived from expression correlations of human neuroblastoma patient samples, we learned specific characteristics of the molecular circuitry of neuroblastoma disease pathogenesis. First, we found that all initial conditions of the wildtype model network led to 36 distinct steady states with p27 activated if and only if trkA was activated in 32 out of 36 states. Second, when we continuously overexpressed or knocked down the expression of trkA or trkB by fixing their model inputs, we could shift the probability of favorable versus unfavorable disease outcomes. Third, when we simulated the model using a realistic 6- gene input signature determined by transcriptome profiling and confirmed by protein expression analysis of the human neuroblastoma SHSY5Y cell line, we found the results accurately predicted disease outcome. Strikingly, our model more accurately predicted the outcomes of 77 young neuroblastoma patients, less than 2 years of age, based on their published 6-gene input signatures.

Manipulation of trkB input dramatically changed the number of steady states suggesting trkB signaling is a critical node of the neuroblastoma pathogenesis molecular network. Overexpression of trkB by fixing trkB 'ON' led to fewer favorable outcomes (53% poor versus 37% good and 10% intermediate) (Fig. 2 and Supplementary Information). This makes logical sense since trkB 'ON' led to activation of mTOR and Proliferation in 18 out of 26 steady states (70%) with a high probability of landing in one of these states. In contrast, knockdown of trkB signaling by fixing trkB 'OFF' led to more favorable disease outcomes. Of interest, only 20% of outcomes gave MYCN 'OFF' when trkB was 'OFF' aligning with literature showing a strong correlation between MYCN amplified metastatic tumors and trkB expression (12, 51). Results showed that overexpression of trkA in silico led to a substantial number (24 out of 32; 75%) of steady states with a favorable outcome (Fig. 2). Furthermore, all steady states had MYCN 'OFF' and p27 'ON', identifiers of less aggressive and more differentiated tumors, respectively (52,53).

Testing the model with a 6-gene input signature derived from the human neuroblastoma SHSY5Y cell line accurately predicted the steady state outcome. Transcriptional profiling determined the 6-gene input signature for the human neuroblastoma SHSY5Y cell line that was confirmed by assessing the 'ON' versus 'OFF' state of each of the 6 input genes signature by protein expression (Fig. 3). When we examined the predicted outcome (Differentiation, 'ON'; Angiogenesis, 'ON'; Apoptosis, 'OFF'; Proliferation, 'OFF') by antibody staining, we confirmed the result (Fig. 3). Together, this confirmed the unfavorable outcome of this cell line and suggested that our model offers a rapid assessment of disease state. That is, human neuroblastoma cell lines or patient derived tissue whose 6-gene input signature is determined by transcriptome and confirmed by protein expression is easily tested in our logic model to rapidly determine the baseline 4 outcome states.

Our model was very successful at predicting the outcome of younger neuroblastoma patients (less than 2 years of age) based on a 6-gene input signature of their patient sample data (Fig. 4). To explain this, we suggest that neuroblastoma cancer in younger patients has a stronger link to developmental signaling pathways (Fig. 4; 91% prediction accuracy) than in older patients (Fig. 4; 55% prediction accuracy). This makes logical sense since neuroblastoma pathogenesis results from inaccuracies in developmental signaling events and these data provide further evidence for targeting developmental genes and signaling pathways in younger patients. Future studies may build on the strength of our logic model as a predictive tool to rapidly assess output states based on the 6-gene input signature derived from human neuroblastoma patient samples. For example, if angiogenesis is a predicted outcome from mTOR activation, then we would suggest that angiogenic inhibitors be added to this patient's therapy regime. If proliferation is activated, then an approach focusing on anti-proliferative agents may be helpful. Alternatively, if differentiation is not observed, then retinoids to induce differentiation may be taken into consideration. By taking the 4 model outcomes into consideration, it is possible to determine the correct balance of therapy for each individual neuroblastoma patient.

In summary, we have gained new insights into the molecular network and predictive value of analyzing a subset of developmental genes and signals involved in neuroblastoma pathogenesis by developing and simulating a logic-based model. The simplicity of a 6-gene input signature and 16 species network allowed us to more easily assess the molecular interactions in the wildtype and manipulated network than other significantly larger gene regulatory networks. The simplicity of the model did not limit the strength of its predictive capability since we more accurately predicted the disease outcome of younger (less than two years of age) neuroblastoma patients than pooled or randomly generated genomic signatures (50). Future studies will exploit this logic model's predictive capabilities and rapidly assess a personalized neuroblastoma patient's molecular circuitry.

Supplementary Material

Refer to Web version on PubMed Central for supplementary material.

Acknowledgments

We thank members of the Histology and Molecular Biology core facilities support at the Stowers Institute for Medical Research.

FUNDING

PMK would like to acknowledge the kind and generous funding from the Stowers Institute for Medical Research, an Alex's Lemonade Stand Foundation Innovation Award, and partial support by the National Institute of Neurological Disorders and Stroke of the National Institutes of Health under Award Number R21NS092001.

References

1. Wei JS, Greer BT, Westermann F, Steinberg SM, Son CG, Chen QR, et al. Prediction of clinical outcome using gene expression profiling and artificial neural networks for patients with neuroblastoma. *Cancer Res.* 2004; 64:6883–6891. [PubMed: 15466177]

2. Schramm A, Schulte JH, Klein-Hitpass L, Havers W, Sieverts H, Berwanger B, et al. Prediction of clinical outcome and biological characterization of neuroblastoma by expression profiling. *Oncogene*. 2005; 24:7902–7912. [PubMed: 16103881]
3. Ohira M, Oba S, Nakamura Y, Isogai E, Kaneko S, Nakagawa A, et al. Expression profiling using tumor-specific cDNA microarray predicts the prognosis of intermediate risk neuroblastoma. *Cancer Cell*. 2005; 7:337–350. [PubMed: 15837623]
4. Oberthuer A, Berthold F, Warnat P, Hero B, Kahlert Y, Spitz R, et al. Customized oligonucleotide microarray gene expression-based classification of neuroblastoma patients outperforms current clinical risk stratification. *J Clin Oncol*. 2006; 24(31):5070–8. [PubMed: 17075126]
5. Fischer M, Oberthuer A, Bror B, Kahlert Y, Skowron M, Voth H, et al. Differential expression of neuronal genes defines subtypes of disseminated neuroblastoma with favorable and unfavorable outcome. *Clin Cancer Res*. 2006; 12:5118–5128. [PubMed: 16951229]
6. Vermeulen J, De Preter K, Naranjo A, Vercruysee L, Van Roy N, Hellemans J, et al. Predicting outcomes for children with neuroblastoma using a multigene-expression signature: a retrospective SIOPEN/COG/GPOH study. 2009; 10:663–671.
7. De Preter K, Vermeulen J, Brors B, Delattre O, Eggert A, Fischer M, et al. Accurate outcome prediction in neuroblastoma across independent data sets using a multigene signature. *Clin Cancer Res*. 2010; 16:1532–1541. [PubMed: 20179214]
8. Formicola D, Petrosino G, Lasorsa VA, Pignataro P, Cimmino F, Vetrella S, et al. An 18 gene expression-based score classifier predicts the clinical outcome in stage 4 neuroblastoma. *J Transl Med*. 2016; 14:142–151. [PubMed: 27188717]
9. Kulesa PM, Lefcort F, Kasemeier-Kulesa JC. The migration of autonomic precursor cells in the embryo. *Auton Neurosci*. 2009; 151(1):3–9. [PubMed: 19783486]
10. Kasemeier-Kulesa JC, Morrison JA, Lefcort F, Kulesa PM. TrkB/BDNF signaling patterns the sympathetic nervous system. *Nat Commun*. 2015; 6:8281. [PubMed: 26404565]
11. Nakagawara A, Azar CG, Scavarda NJ, Brodeur GM. Expression and function of TRK-B and BDNF in human neuroblastomas. *Mol Cell Biol*. 1994; 14:759–767. [PubMed: 8264643]
12. Brodeur GM, Minturn JE, Ho R, Simpson AM, Iyer R, Varela CR, et al. Trk receptor expression and inhibition in neuroblastomas. *Clin Cancer Res*. 2009; 15:3244–3250. [PubMed: 19417027]
13. Reiff T, Huber L, Kramer M, Delattre O, Janoueix-Lerouet I, Rohrer H. Midkine and Alk signaling in sympathetic neuron proliferation and neuroblastoma predisposition. *Dev*. 2011; 138:4699–4708.
14. De Brouwer S, De Preter K, Kumps C, Zabrocki P, Porcu M, Westerhout, et al. Meta-analysis of neuroblastoma reveals a skewed ALK mutation spectrum in tumors with MYCN amplification. *Clin Cancer Res*. 2010; 16:4353–4362. [PubMed: 20719933]
15. Schulte JH, Bachmann HS, Brockmeyer B, DePreter K, Oberthuer A, Ackermann S, et al. High ALK receptor tyrosine kinase expression supersedes ALK mutation as a determining factor of an unfavorable phenotype in primary neuroblastoma. *Clin Cancer Res*. 2011; 17:5082–5092. [PubMed: 21632861]
16. Kramer M, Ribeiro D, Arsenian-Henriksson M, Deller T, Rohrer H. Proliferation and survival of embryonic sympathetic neuroblasts by MYCN and activated ALK signaling. *J Neurosci*. 2016; 36:10425–10439. [PubMed: 27707976]
17. Brodeur GM, Bagatell R. Mechanisms of neuroblastoma regression. *Nat Rev Clin Oncol*. 2014; 11:704–713. [PubMed: 25331179]
18. Bornholdt S. Boolean network models of cellular regulation: prospects and limitations. *J R Soc Interface*. 2008; 5:S85–94. [PubMed: 18508746]
19. Wynn ML, Consul N, Merajver SD, Schnell S. Inferring the effects of honokiol on the notch signaling pathway in SW480 colon cancer cells. *Cancer Inform*. 2014; 13:1–12.
20. Saez-Rodriguez J, Simeoni L, Lindquist JA, Hemenway R, Bommhardt U, Arndt B, et al. A logical model provides insight into T cell receptor signaling. *PLoS Comput Biol*. 2007; 3:e163. [PubMed: 17722974]
21. Sahin O, Frohlich H, Lobke C, Korf U, Burmester S, Majesty M, et al. Modeling ERBB receptor-regulated G1/S transition to find novel targets for de novo trastuzumab resistance. *BMC Syst Biol*. 2009; 3:1. [PubMed: 19118495]

22. Samaga R, Saez-Rodriguez J, Alexopoulos LG, Sorger PK, Klamt S. The logic of EGFR/ErbB signaling: theoretical properties and analysis of high-throughput data. *PLoS Comput Biol*. 2009; 5:e1000438. [PubMed: 19662154]
23. Ryll A, Samaga R, Schaper F, Alexopoulos LG, Klamt S. Large-scale models of IL-1 and IL-6 signaling and their hepatocellular specification. *Mol Biosyst*. 2011; 7:3253–3270. [PubMed: 21968890]
24. Li F, Long T, Lu Y, Ouyang Q, Tang C. The yeast cell-cycle network is robustly designed. *Proc Natl Acad Sci USA*. 2004; 100:4781–4786.
25. Albert R, Othmer HG. The topology of the regulatory interactions predicts the expression pattern of the segment polarity genes in *Drosophila melanogaster*. *J Theor Biol*. 2003; 223:1–18. [PubMed: 12782112]
26. Szallasi Z, Liang S. Modeling the normal and neoplastic cell cycle with “realistic Boolean genetic networks”: their application for understanding carcinogenesis and assessing therapeutic strategies. *Pac Symp Biocomput*. 1998:66–76. [PubMed: 9697172]
27. Thomas R, Thieffry D, Kaufman M. Dynamical behavior of biological regulator networks—I. Biological role of feedback loops and practical use of the concept of the loop-characteristic state. *Bull Math Biol*. 1995; 57:247–276. [PubMed: 7703920]
28. Wang Q, Diskin S, Rappaport E, Attiyeh E, Mosse Y, Shue D, et al. Integrative genomics identifies distinct molecular classes of neuroblastoma and shows that multiple genes are targeted by regional alternations in DNA copy number. 2006; 66:6050–6062.
29. Wynn ML, Consul N, Merajver SD, Schnell S. Logic-based models in systems biology: a predictive and parameter-free network analysis method. *Integr Biol (Camb)*. 2012; 4:1323–1337. [PubMed: 23072820]
30. Nakaguro M, Kiyonari S, Kishida S, Cao D, Murakami-Tonami Y, Ichikawa H, et al. Nucleolar protein PES1 is a marker of neuroblastoma outcome and is associated with neuroblastoma differentiation. *Cancer Science*. 2015; 106:237–243. [PubMed: 25557119]
31. Puppo M, Pastorino S, Melillo G, Pezzolo A, Varesio L, Bosco MC. Induction of apoptosis by flavopiridol in human neuroblastoma cells is enhanced under hypoxia and associated with N-myc proto-oncogene down-regulation. *Clin Cancer Res*. 2004; 10:8704–8719. [PubMed: 15623656]
32. Tan C, Cruet-Hennequart S, Troussard A, Fazil L, Costello P, Sutton K, et al. Regulation of tumor angiogenesis by integrin-linked kinase (ILK). *Cancer Cell*. 2004; 5:79–90. [PubMed: 14749128]
33. Zha Y, Xia Y, Ding J, Choi J-H, Yang L, Dong Z, et al. MEIS2 is essential for neuroblastoma cell survival and proliferation by transcriptional control of M-phase progression. *Cell Death and Disease*. 2014; 5:e1417. [PubMed: 25210800]
34. Rifkin JT, Todd VJ, Anderson LW, Lefcort F. Dynamic expression of neurotrophin receptors during sensory neuron genesis and differentiation. *Dev Biol*. 2000; 227:465–480. [PubMed: 11071767]
35. Kasemeier-Kulesa JC, Bradley R, Pasquale EB, Lefcort F, Kulesa PM. Eph/ephrins and N-cadherin coordinate to control the pattern of sympathetic ganglia. *Dev*. 2006; 133(24):4839–47.
36. Kasemeier-Kulesa JC, Kulesa PM, Lefcort F. Imaging neural crest cell dynamics during formation of dorsal root ganglia and sympathetic ganglia. *Dev*. 2005; 132(2):235–45.
37. Qayed M, Chiang KY, Ricketts R, Alazraki A, Tahvildari A, Haight A, George B, Esiashvili N, Katzenstein HM. Tandem stem cell rescue as consolidation therapy for high-risk neuroblastoma. *Pediatr Blood Cancer*. 2012 Mar; 58(3):448–52. [PubMed: 21538822]
38. Kolch W. Coordinating ERK/MAPK signaling through scaffolds and inhibitors. *Nat Rev Mol Cell Biol*. 2005 Nov; 6(11):827–37. [PubMed: 16227978]
39. Shaul YD, Seger R. The MEK/ERK cascade: from signaling specificity to diverse functions. *Biochim Biophys Acta*. 2007 Aug; 1773(8):1213–26. [PubMed: 17112607]
40. Griner EM, Kazanietz MG. Protein kinases C and other diacylglycerol effectors in cancer. *Nat Rev Cancer*. 2007 Apr; 7(4):281–94. [PubMed: 17384583]
41. Qiao J, Paul P, Lee S, Qiao L, Josifi E, Tiao JR, Chung DH. PI3K/AKT and ERK regulate retinoic acid-induced neuroblastoma cellular differentiation. *Biochem Biophys Res Commun*. 2012 Aug 3; 424(3):421–6. [PubMed: 22766505]
42. Huang EJ, Reichardt LF. Neurotrophins: roles in neuronal development and function. *Annu Rev Neurosci*. 2001; 24:677–736. [PubMed: 11520916]

43. Chao MV. Neurotrophins and their receptors: a convergence point for many signaling pathways. *Nat Rev Neurosci*. 2003 Apr; 4(4):299–309. [PubMed: 12671646]
44. Mei H, Wang Y, Lin Z, Tong Q. The mTOR signaling pathway in pediatric neuroblastoma. *Pediatr Hematol Oncol*. 2013 Oct; 30(7):605–15. [PubMed: 23697980]
45. Kang J, Rychahou PG, Ishola TA, Mourot JM, Evers BM, Chung DH. *Oncogene*. 2008 Jun; 26(28):27. 3999–4007.
46. Segerstrom L, Baryawno N, Sveinbjornsson B, Wickstrom M, Elfman L, Kogner P, Johnsen JJ. Effects of small molecule inhibitors of PI3K/Akt/mTOR signaling on neuroblastoma growth in vitro and in vivo. *Int J Cancer*. 2011 Dec 15; 129(12):2958–65. [PubMed: 21717457]
47. Chanthery YH, Gustafson WC, Itsara M, Persson A, Hackett CS, Grimmer M, Charron E, Yakovenko S, Kim G, Matthay KK. Paracrine signaling through MYCN enhances tumor-vascular interactions in neuroblastoma. *Sci Transl Med*. 2012; 4:115ra3.
48. Huang M, Weiss WA. Neuroblastoma and MYCN. *Cold Spring Harb Perspect Med*. 2013 Oct 1; 3(10):1–22.
49. Mei Y, Wang Z, Zhang L, Zhang Y, Li X, Liu H, et al. Regulation of neuroblastoma differentiation by forkhead transcription factors FOXO1/3/4 through the receptor tyrosine kinase PDGFRA. *PNAS*. 2012; 109:4898–4903. [PubMed: 22411791]
50. Hallett RM, Seong AB, Kaplan DR, Irwin MS. Transcript signatures that predict outcome and identify targetable pathways in MYCN-amplified neuroblastoma. 2016; 10:1461–1472.
51. Edsjo A, Lavenius E, Nilsson H, Hoehner JC, Simonsson P, Culp LA, et al. Expression of trkB in human neuroblastoma in relations to MYCN expression and retinoic acid treatment. *Lab Invest*. 2003; N83:813–823.
52. Kaneko Y, Suenaga Y, Islam SM, Matsumoto D, Makamura Y, Ohira M, et al. Functional interplay between MYCN, NCYM, and OCT4 promotes aggressiveness of human neuroblastomas. *Cancer Sci*. 2015; 106:840–847. [PubMed: 25880909]
53. Nakamura Y, Ozaki T, Koseki H, Nakagawara A, Sakiyama S. Accumulation of p27 KIP1 is associated with BMP2-induced growth arrest and neuronal differentiation of human neuroblastoma-derived cell lines. *Biochem Biophys Res Commun*. 2003; 307:203–213.

- We construct and simulate a molecular network model of neuroblastoma
- This logic model uses a 6-gene input to predict outcome of four cell states
- The four cell states predict favorable/unfavorable neuroblastoma outcome
- We simulate the mis-expression of tyrosine receptor kinases trkA and trkB
- trkA and trkB are prognostic indicators of neuroblastoma
- We validate the model using RNAseq of SHSY5Y human neuroblastoma cell line
- We use 77 published human patient sample signatures to predict disease outcome
- The model is a more accurate predictor of early stage disease than any current gene list

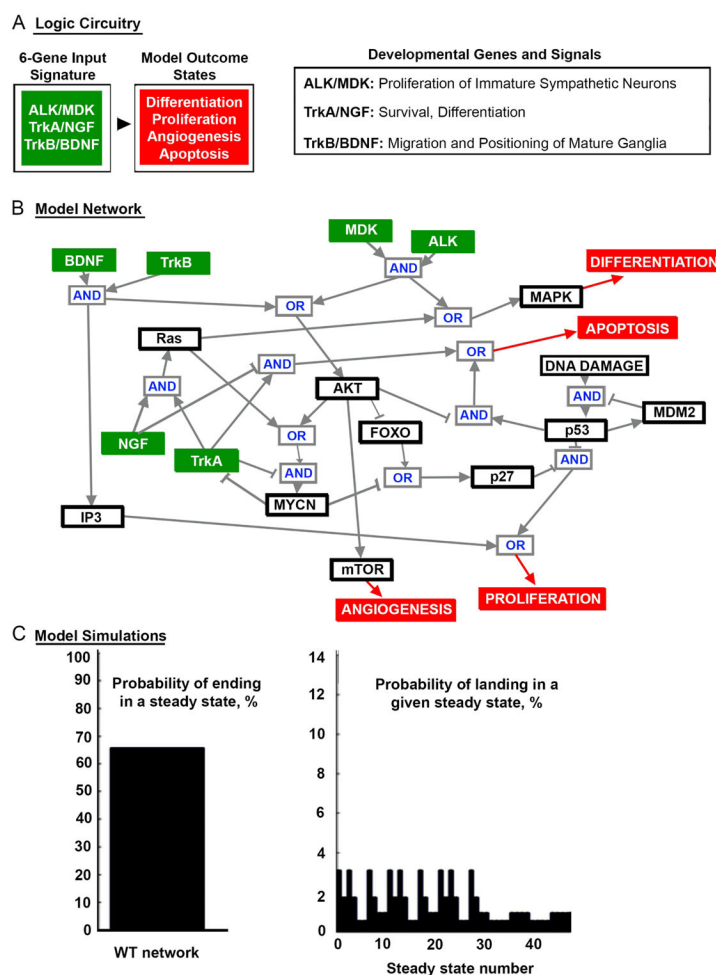


Figure 1. Development of logic model to predict neuroblastoma states

A. Logic model inputs (green) included the tyrosine kinase receptor/ligand pairs ALK/MDK; trkA/NGF and trkB/BDNF, and model outcomes states (red) included differentiation, proliferation, angiogenesis and apoptosis. B. Logic model construction using ‘AND’ and ‘OR’ gates. Green boxes indicate input genes, red boxes indicate output states, black boxes indicate gene nodes in network, grey boxes indicate AND/OR gates. C. Graph on left shows the probability of ending in a steady state using the wild-type network (shown in B). Graph on right shows the probability (percent chance) of ending in the different steady states generated by the model (1–46).

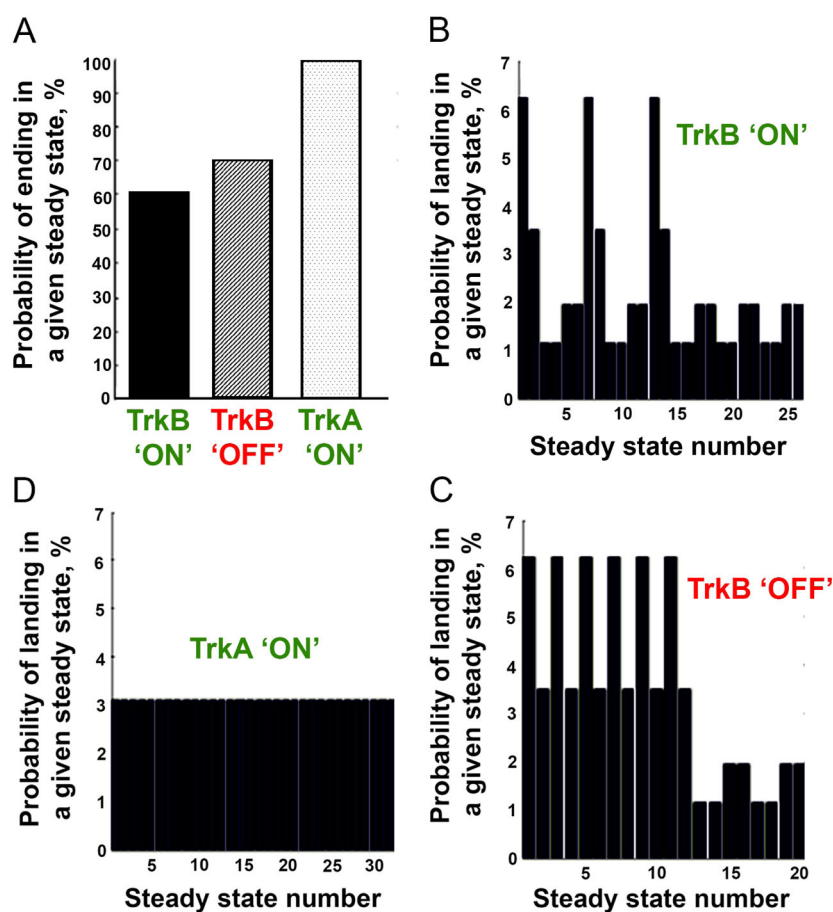


Figure 2. Perturbations to the network alter steady state distribution

A. Probability of ending in a given state when *trkB* is fixed 'ON' (60%; black bar), *trkB* is fixed 'OFF' (70%; dashed bar) and *trkA* is fixed 'ON' (100%; dotted bar). B–D. The distribution of the probability of landing in each steady state generated when (B) *trkB* is fixed 'ON' (n=26 possible steady states); (C) *trkB* is fixed 'OFF' (n=20 possible steady states); and (D) when *trkA* is fixed 'ON' (32 possible steady states).

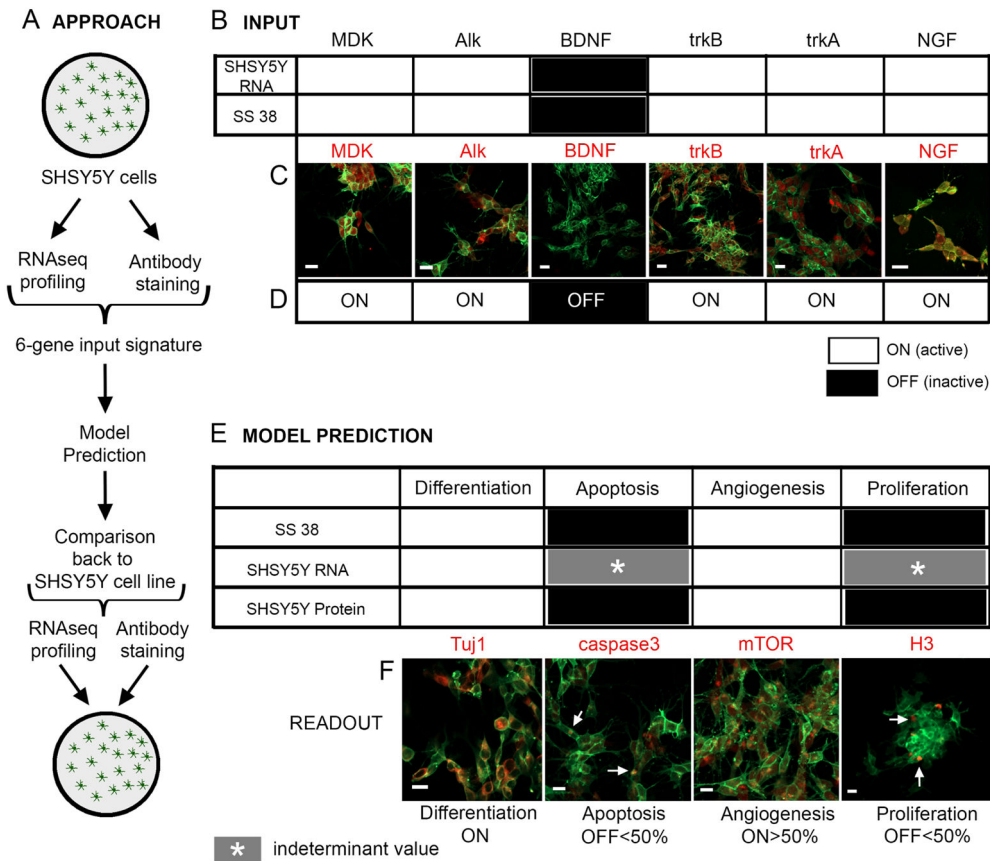


Figure 3. Application of logic model to the neuroblastoma cell line SHSY5Y

A. Schematic of workflow showing SHSY5Y cells were analyzed for the 6-gene input signature using RNAseq and Antibody staining, which were then put into the logic model to predict the output states. These predictions were then confirmed using both RNAseq and protein expression. B. 6-gene input signature expression based on SHSY5Y RNAseq data (top row) compared to the predicted state from the logic model (steady state 38; bottom row). White bare indicated ON (active state) and black bar indicated OFF (inactive state). C. Antibody expression (red) of the 6-gene input signature on SHSY5Y cells (green) in culture: MDK, ALK, BDNF, trkB, trkA and NGF. D. Input signature genes from logic model, SHSY5Y RNA and SHSY5Y antibody stains are similar. E. Model predictions (differentiation, apoptosis, angiogenesis and proliferation) for steady state 38 (top row), SHSY5Y RNA and SHSY5Y antibody protein expression. Asterisk/grey bar indicated indeterminant value based on inconclusive RNAseq value. F. Antibody expression of markers for the 4 readout states (red) on SHSY5Y cells (green). Scale bars=10um in C and F.

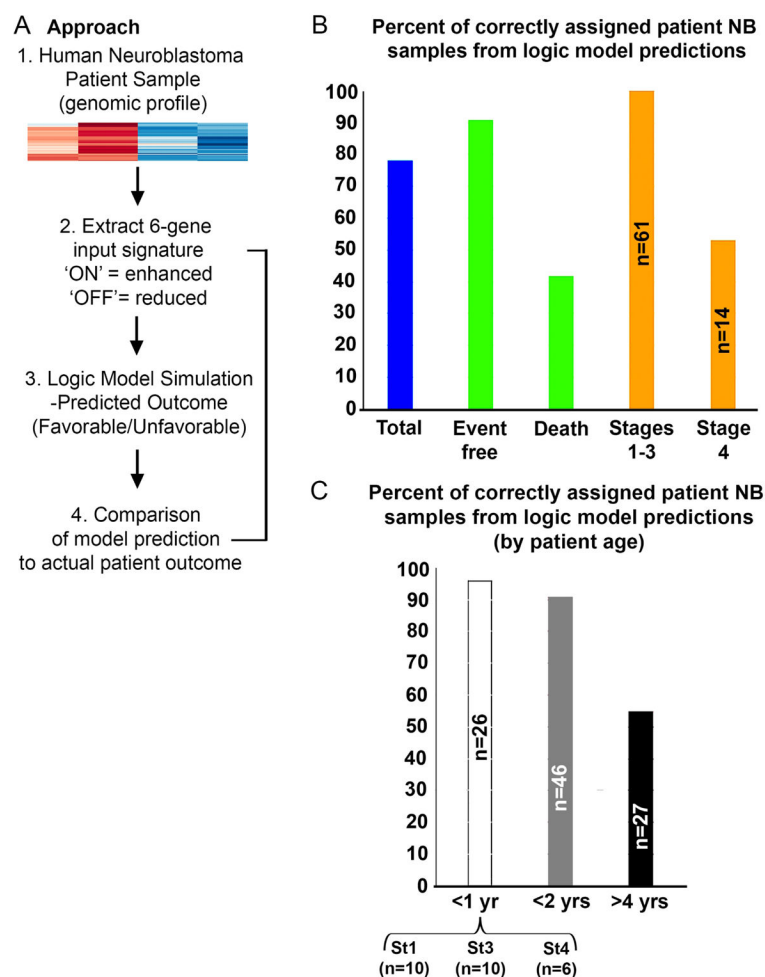


Figure 4. Application of Logic model to mined patient sample data

A. Workflow of mining genomic profile of human neuroblastoma patient samples for the 6-gene input signature, using the logic model to predict outcome and comparing it to known patient data outcome. B. Graph of the percent of correctly assigned patient neuroblastoma samples from logic model predictions. 78% of all patient samples were correctly predict (blue bar). Subcategorizing the patient samples gave the following correct predictions: 91% of event free patients (green) and 42% of death patients (green); 100% of stage 1–3 neuroblastomas (orange, n=61 patients) and 53% of stage 4 neuroblastomas (orange, n=14 patients). C. The entire patient sample study was further analyzed based on age of patient with 96% accuracy rate of prediction for patients <1 year of age (white bar, n=26 patients: 10 stage 1, 10 stage 3 and 6 stage 4), 91% accuracy for patients <2 years of age (grey bar) and 55% accuracy for patients >4 years of age (black bar).

Table 1

Indication of logic functions.

Rule Number	Node	Regulation rule
1	TrkB	$\text{TrkB}^{t+1} = \text{TrkB}^t$
2	BDNF	$\text{BDNF}^{t+1} = \text{BDNF}^t$
3	TrkA	$\text{TrkA}^{t+1} = \text{NOT MYCN}^t$
4	NGF	$\text{NGF}^{t+1} = \text{NGF}^t$
5	MDK	$\text{MDK}^{t+1} = \text{MDK}^t$
6	ALK	$\text{ALK}^{t+1} = \text{ALK}^t$
7	Ras	$\text{Ras}^{t+1} = \text{NGF}^t \text{ AND } \text{TrkA}^t$
8	AKT	$\text{AKT}^{t+1} = (\text{BDNF}^t \text{ AND } \text{TrkB}^t) \text{ OR } (\text{MDK}^t \text{ AND } \text{ALK}^t)$
9	MYCN	$\text{MYCN}^{t+1} = (\text{Ras}^t \text{ or } \text{AKT}^t) \text{ and not } \text{TrkA}^t$
10	FOXO	$\text{FOXO}^{t+1} = \text{not } \text{AKT}^t$
11	p27	$\text{p27}^{t+1} = \text{FOXO}^t \text{ OR } (\text{NOT MYCN}^t)$
12	p53	$\text{p53}^{t+1} = \text{p53}^t$
13	MDM2	$\text{MDM2}^{t+1} = \text{p53}^t$
14	IP3	$\text{IP3}^{t+1} = \text{BDNF}^t \text{ AND } \text{TrkB}^t$
15	Differentiation	$\text{Differentiation}^{t+1} = \text{Ras}^t \text{ OR } (\text{MDK}^t \text{ AND } \text{ALK}^t)$
16	Apoptosis	$\text{Apoptosis}^{t+1} = (\text{p53}^t \text{ AND NOT } \text{AKT}^t) \text{ OR } (\text{TrkA}^t \text{ AND NOT } \text{NGF}^t)$
17	Angiogenesis	$\text{Angiogenesis}^{t+1} = \text{AKT}^t$
18	Proliferation	$\text{Proliferation}^{t+1} = \text{IP3}^t \text{ OR } (\text{NOT } \text{p27}^t \text{ AND NOT } \text{p53}^t)$